Learning to Beamform for Integrated Sensing and Communication: A Graph Neural Network with Implicit Projection Approach

Yifei Zhao, Yong Zhou, *Senior Member, IEEE*, Zixin Wang, *Member, IEEE*, Yuanming Shi, *Senior Member, IEEE*, Nan Cheng, *Senior Member, IEEE*, and Haibo Zhou, *Senior Member, IEEE*

***Abstract*—Integrated sensing and communication (ISAC), as an important usage scenario of 6G, is capable of seamlessly integrating wireless sensing and communication for their mutual benefit. Taking full advantage of ISAC heavily relies on effectively solving resource allocation problems, which, however, are generally high-dimensional and non-convex, resulting in the optimization-based algorithms exhibiting high computation complexity and the traditional learning-based algorithms returning infeasible solutions. In this paper, we consider an ISAC scenario featured by multiple communication users and multiple sensing targets, aiming to develop an efficient and scalable algorithm that optimizes the radar transmit beampattern under the communication performance constraint. To this end, we propose a graph neural network (GNN) with implicit projection framework, where GNN captures the intricate interactions between communication users and sensing targets and meanwhile enables the joint optimization of communication and sensing beamforming matrices, and the projection module is applied to ensure the feasibility of the beamforming matrices design. Via capturing the permutation equivalence for communication matrices and the permutation invariance for the sensing matrix, the scalability of the proposed algorithm is guaranteed. Simulation results show that the proposed algorithm significantly reduces the computation complexity compared to the baselines, and achieves excellent algorithmic scalability and constraint satisfaction.**

***Index Terms*—Integrated sensing and communication, graph neural network, implicit projection.**

I. Introduction

Recognized by International Telecommunication Union (ITU) as an important usage scenario of 6G, integrated sensing and communication (ISAC) aims to achieve seamless integration of wireless sensing and communication functions while pursuing mutual gains in their performance. Compared to the separate design of communication and sensing processes, ISAC has the advantages of achieving higher spectrum, power, and hardware utilization via jointly optimizing the communication and sensing waveforms and resources [1]. With these advantages, ISAC has a wide range of applications in the fields of autonomous driving, smart city, remote sensing, and environmental monitoring [2], [3].

Waveform design is an essential aspect for unleashing the full potential of ISAC, which can be divided into sensing-centric design (SCD), communication-centric design (CCD), and joint design (JD) [1], [4]. SCD aims at integrating communication functions into existing sensing waveforms, where the radar signal remains unchanged and the primary focus is on the sensing function. For example, the authors in [5], [6] propose to embed the communication signals into the chirp signals to generate the ISAC waveform, while the authors in [7] implement the communication functionality by shuffling the waveforms across multiple transmit antennas. Different from SCD, CCD achieves the sensing function through the existing communication waveforms while prioritizing the communication performance. For instance, the authors in [8], [9] employ orthogonal frequency division multiplexing (OFDM) waveforms for radar sensing, aiming to optimally implement the radar sensing function while minimizing its impact on communication performance. Moreover, the authors in [10]–[13] use the JD approach to balance the performance tradeoff between sensing and communication. As the resource allocation problem for ISAC is generally high-dimensional and non-convex, the traditional optimization-based methods typically require high computation complexity without being able to obtain optimal solutions.

Machine learning (ML) has the potential to achieve low-complexity resource allocation after being well-trained, given its unique feature of achieving nonlinear mapping [14]–[16], making it suitable for efficiently solving high-dimensional non-convex optimization problems [17]–[20]. As a result, the paradigm of learning-to-optimize has been increasingly explored in ISAC. In particular, the authors in [21] develop a long short-term memory (LSTM) network for predictive beamforming in ISAC-based vehicle-to-infrastructure (V2I) networks. This method does not require an explicit channel tracking process and significantly reduces the signaling overhead. While in [22], the authors propose an end-to-end approach that directly maps the pilot signals to the beamforming matrices to perform ISAC. In addition, the authors in [23] propose unsupervised

The work of Yong Zhou was supported by the Natural Science Foundation of Shanghai under Grant 23ZR1442800. The work of Yuanming Shi was supported in part by the National Nature Science Foundation of China under Grant 62271318 and the Shanghai Rising-Star Program under Grant No. 22QA1406100. (*Corresponding author: Yong Zhou.*)

Y. Zhao, Y. Zhou, and Y. Shi are with the School of Information Science and Technology, ShanghaiTech University, Shanghai 201210, China (e-mail: zhaoyf@shanghaitech.edu.cn; zhouyong@shanghaitech; shiym@shanghaitech.edu.cn).

Z. Wang is with the Department of Electronic and Computer Engineering, The Hong Kong University of Science and Technology, Hong Kong (e-mail: eewangzx@ust.hk).

N. Cheng is with the State Key Laboratory of ISN and the School of Telecommunications Engineering, Xidian University, Xi'an 710071, China (e-mail: dr.nan.cheng@ieee.org).

H. Zhou is with the School of Electronic Science and Engineering, Nanjing University, Nanjing 210023, China (e-mail: haibozhou@nju.edu.cn).

learning methods for interference management, while avoiding high computation complexity incurred by optimization-based methods.

Although promising, the ML-based algorithm still encounters the following challenges. First, conventional fully-connected neural networks (FCNNs) are unable to effectively utilize the spatial interaction between sensing and communication devices in ISAC systems. Fortunately, such spatial interaction can be captured and leveraged by graph neural network (GNN) to enhance the performance of ISAC. Additionally, GNN possesses unique features of permutation invariance and permutation equivalence [24]–[26], which set it apart from FCNNs and enable excellent algorithmic scalability. In particular, the authors in [26] consider a communication system involving intelligent reflective surface (IRS) and develop a GNN containing user nodes and IRS nodes to learn mapping from the received pilots to an optimized system configuration. Nevertheless, the GNN in [26] cannot be directly applied to ISAC scenarios due to the absence of sensing node design as well as complex communication or sensing constraints.. Second, the solutions returned by conventional data-driven learning algorithms are not guaranteed to satisfy the stringent non-convex constraints. Although normalization and Newton's method can be applied to tackle simple constraints (e.g., the maximum transmit power constraint), the constraints of resource allocation problems in ISAC scenarios are often associated with sensing and/or communication performance and take on a nonlinear and non-convex form of high complexity. Under this circumstance, the penalty-based approach widely used in the learning algorithm, which converts constraints into penalty terms in the loss function, has a high probability of producing infeasible solutions for stringent performance constraints, owing to the lack of strict constraint enforcement. Designing an effective learning framework that comprehensively tackles the aforementioned challenges while considering the unique features of ISAC is crucial but has not been investigated yet, and this serves as the primary motivation behind our work.

In this paper, we consider an ISAC system, where the base station (BS) simultaneously performs sensing of multiple targets and communicates with multiple communication users. Our objective is to develop an efficient and scalable algorithm that optimizes the radar transmit beampattern under the constraint of communication performance. To achieve this objective, we propose a novel GNN with implicit projection (GNN-IP) algorithm to achieve scalable and feasible beamforming design. To summarize, this paper presents the following contributions:

1) For an ISAC model involving multiple communication users and sensing targets, we design a GNN module to construct a mapping from the communication and sensing channel state information (CSI) to the transmit beamforming matrices. Our proposed GNN architecture captures the intricate interactions between communication users and sensing targets, enabling the joint optimization of communication and sensing transmit waveforms. Meanwhile, the GNN's permutation equivalence for communication matrices and permutation invariance for the sensing matrix ensure its scalability with respect to the number of communication users.

2) To ensure the feasibility of the beamforming matrices design, we introduce a differentiable projection module. When the solution returned by the GNN module does not satisfy the constraints, the proposed projection module projects the output of the GNN to the feasible set defined by the communication performance and transmit power constraints. Therefore, the proposed GNN-IP algorithm is capable of ensuring the feasibility of stringent communication performance constraints, while achieving excellent sensing performance.

3) The simulation results show that the proposed GNN-IP algorithm exhibits significantly reduced computation complexity compared to the conventional optimization-based algorithms, while still approaching similar sensing mean-squared error (MSE) performance. Additionally, our proposed algorithm demonstrates substantial enhancements in both sensing performance and constraint satisfaction when compared to the conventional FCNNs.

The rest of the paper is organized as follows. In Section II, we present the system model and problem formulation of ISAC systems under consideration. Section III describes the proposed GNN-IP architecture. Section IV presents the simulation results. Finally, Section V concludes this paper.

Notations: In this paper, $(\cdot)^{\mathrm{T}}$ and $(\cdot)^{\mathrm{H}}$ denote transpose and Hermitian, respectively. Vectors are represented by bold lower class letters, and matrices are represented by bold upper class letters. We denote $\mathbf{0}^{m\times n}$ as the $m \times n$ zero matrix. $\mathbb{E}$ denotes the stochastic expectation. $\mathrm{Tr}(\cdot)$ and $\mathrm{rank}(\cdot)$ denote the trace and rank for the matrix, respectively.

II. System Model and Problem Formulation

In this section, we present the system model of ISAC, including the sensing and communication models, and construct a resource allocation problem for minimizing the sensing MSE.

A. System Model

Consider an ISAC system, where a BS equipped with a uniform linear array (ULA) consisting of M half-wavelength spaced antennas simultaneously communicates with L downlink users ($L \leq M$) indexed by $\mathcal{L} = \{1, \ldots, L\}$ and meanwhile detects K radar targets ($K \leq M$) indexed by $\mathcal{K} = \{1, \ldots, K\}$, as shown in Fig. 1.

We denote the L parallel data streams from the BS to the users as $\boldsymbol{d} = [d_1, d_2, \ldots, d_L]^{\mathrm{T}}$ and the corresponding communication beamforming matrix at the BS as $\boldsymbol{C} = [\boldsymbol{c}_1, \boldsymbol{c}_2, \ldots, \boldsymbol{c}_L] \in \mathbb{C}^{M\times L}$. Meanwhile, to maximize the degrees of freedom (DoF) of the sensing waveform, we denote the individual sensing symbols and the corresponding sensing beamforming matrix as $\boldsymbol{w} = [w_1, w_2, \cdots, w_M]^{\mathrm{T}}$ and $\boldsymbol{S} = [\boldsymbol{s}_1, \boldsymbol{s}_2, \cdots, \boldsymbol{s}_M] \in \mathbb{C}^{M\times M}$, respectively. Hence, the transmit signal for joint sensing and communication at the BS can be expressed as

$$\boldsymbol{x} = \boldsymbol{C}\boldsymbol{d} + \boldsymbol{S}\boldsymbol{w}. \tag{1}$$

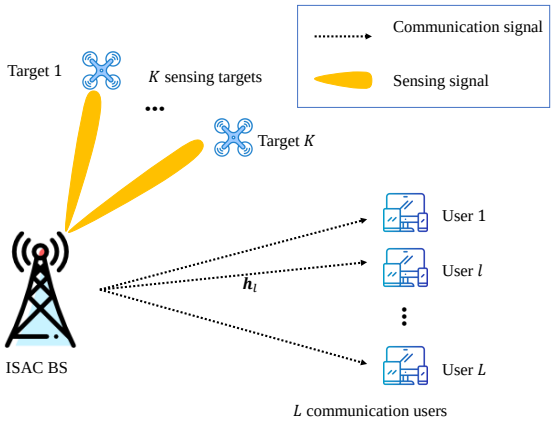

Fig. 1. An illustration of ISAC system with K radar targets and L communication users.

Without loss of generality, we assume that the data streams of different users are independent of each other and independent from the radar symbols as in [27]–[29], i.e.,

$$\mathbb{E}\left(\boldsymbol{d}\boldsymbol{w}^{\mathrm{H}}\right)=\mathbf{0}^{L\times M}, \tag{2}$$

and the communication and sensing symbols have unit power, i.e.,

$$\mathbb{E}\left(\boldsymbol{d}\boldsymbol{d}^{\mathrm{H}}\right)=\mathbb{E}\left(\boldsymbol{w}\boldsymbol{w}^{\mathrm{H}}\right)=\boldsymbol{I}. \tag{3}$$

Given the maximum transmit power budget P_0 at the BS, we have

$$\mathbb{E}\left(\|\boldsymbol{x}\|^2\right)=\mathrm{Tr}\left(\boldsymbol{R}\right)=\mathrm{Tr}\left(\boldsymbol{C}\boldsymbol{C}^{\mathrm{H}}+\boldsymbol{S}\boldsymbol{S}^{\mathrm{H}}\right)\leq P_0, \tag{4}$$

where $\boldsymbol{R}=\boldsymbol{C}\boldsymbol{C}^{\mathrm{H}}+\boldsymbol{S}\boldsymbol{S}^{\mathrm{H}}$ is the covariance matrix of the transmit signal.

In the following, we shall elaborate the radar sensing model and communication model.

1) Radar Sensing Model: We consider a radar probing scenario [30]–[33] where the main objective is to direct the transmit beam toward specific given directions to obtain more information about the illuminated target. These directions are typically known to the transmitter. For instance, the beam direction is given by the center of the angular sector of interest in searching mode and determined by the observed directions of previous targets in tracking mode.

Following [34], [35], we consider that both the communication and sensing signals are utilized in target sensing. The signal at angular position θ can be expressed as

$$z(\theta)=\boldsymbol{a}^{\mathrm{H}}(\theta)\boldsymbol{x}, \tag{5}$$

where $\boldsymbol{a}(\theta)$ is the array response vector. By denoting Δ as the normalized antenna interval, $\boldsymbol{a}(\theta)$ can be written as $\boldsymbol{a}(\theta)=[1,\ldots,e^{-j2\pi(M-1)\Delta\sin\theta}]^{\mathrm{T}}$. We aim to maximize the energy of sensing signal towards the designated direction via aligning the transmitted signal with the desired beampattern. Specifically, the beampattern at a given angular position θ can be represented as

$$P(\theta;\boldsymbol{R})=\mathbb{E}(|z(\theta)|^2)=\boldsymbol{a}^{\mathrm{H}}(\theta)\boldsymbol{R}\boldsymbol{a}(\theta). \tag{6}$$

As in [32], [33], we evaluate the sensing performance by measuring the MSE between the desired and obtained beampatterns, which can be expressed as

$$L(\boldsymbol{R})=\frac{1}{N}\sum_{n=1}^{N}|\beta b(\theta_n)-P(\theta_n;\boldsymbol{R})|^2, \tag{7}$$

where $b(\theta)$ is the desired beampattern for angle θ, β is the power normalization parameter, $\{\theta_n\}_{n=1}^N$ denote the fine grid of points that cover the entire location sector of the sensing targets, and N is the total number of sample grids.

2) Communication Model: We assume that the channel state information between the BS and the communication user is available and can be obtained by various state-of-the-art channel estimation algorithms. By denoting the channel vector from the BS to user l as $\boldsymbol{h}_l$, the received signal at user l is

$$\begin{aligned} r_l&=\boldsymbol{h}_l^{\mathrm{H}}\boldsymbol{x}+n_l\\ &=\boldsymbol{h}_l^{\mathrm{H}}\left(\boldsymbol{c}_l d_l+\sum_{j=1,j\neq l}^{L}\boldsymbol{c}_j d_j+\sum_{i=1}^{M}\boldsymbol{s}_i w_m\right)+n_l, \end{aligned} \tag{8}$$

where n_l is the additive white Gaussian noise (AWGN) with zero mean and variance σ^2. In particular, $\boldsymbol{c}_l d_l$ is the intended signal received by the l-th user, $\sum_{j=1,j\neq l}^{L}\boldsymbol{c}_j d_j$ is the interference from multi-user communication, and $\sum_{i=1}^{M}\boldsymbol{s}_i w_m$ is the interference caused by sensing signals. Therefore, the signal-to-interference-plus-noise ratio (SINR) of the l-th user, denoted as Γ_l, can be expressed as

$$\begin{aligned} \Gamma_l&=\frac{\left|\boldsymbol{h}_l^{\mathrm{H}}\boldsymbol{c}_l\right|^2}{\sum_{j=1,j\neq l}^{L}\left|\boldsymbol{h}_l^{\mathrm{H}}\boldsymbol{c}_j\right|^2+\sum_{i=1}^{M}\left|\boldsymbol{h}_l^{\mathrm{H}}\boldsymbol{s}_i\right|^2+\sigma^2}\\ &=\frac{\boldsymbol{h}_l^{\mathrm{H}}\boldsymbol{c}_l\boldsymbol{c}_l^{\mathrm{H}}\boldsymbol{h}_l}{\boldsymbol{h}_l^{\mathrm{H}}\left(\sum_{j=1,j\neq l}^{L}\boldsymbol{c}_j\boldsymbol{c}_j^{\mathrm{H}}+\boldsymbol{S}\boldsymbol{S}^{\mathrm{H}}\right)\boldsymbol{h}_l+\sigma^2}\\ &=\frac{\boldsymbol{h}_l^{\mathrm{H}}\boldsymbol{C}_l\boldsymbol{h}_l}{\boldsymbol{h}_l^{\mathrm{H}}\left(\boldsymbol{R}-\boldsymbol{C}_l\right)\boldsymbol{h}_l+\sigma^2}, \end{aligned} \tag{9}$$

where $\boldsymbol{C}_l=\boldsymbol{c}_l\boldsymbol{c}_l^{\mathrm{H}}$.

To ensure the communication performance for each user, a minimum SINR threshold, denoted as Γ_0, for each communication user should be satisfied, i.e.,

$$\Gamma_l\geq\Gamma_0,\forall\, l\in\mathcal{L}. \tag{10}$$

B. Problem Formulation

We aim to develop a computation-efficient algorithm that minimizes $L(\boldsymbol{R})$ while ensuring the communication SINR for each user. The designed transmit waveform should maximize the main lobes energy towards the sensing targets as well as the communication users, while suppressing the side lobes energy. The joint optimization problem can be formulated as

$$\underset{\boldsymbol{C}_1,\ldots,\boldsymbol{C}_L,\boldsymbol{S}}{\text{minimize}}\quad L(\boldsymbol{R}) \tag{11a}$$

$$\text{subject to}\ \ \boldsymbol{R}=\sum_{l=1}^{L}\boldsymbol{C}_l+\boldsymbol{S}\boldsymbol{S}^{\mathrm{H}}\succeq 0, \tag{11b}$$

$$\mathrm{Tr}(\boldsymbol{R})=P_0, \tag{11c}$$

$$\mathrm{rank}(\boldsymbol{C}_l)=1,\forall\, l\in\mathcal{L}, \tag{11d}$$

$$\Gamma_l\geq\Gamma_0,\forall\, l\in\mathcal{L}, \tag{11e}$$

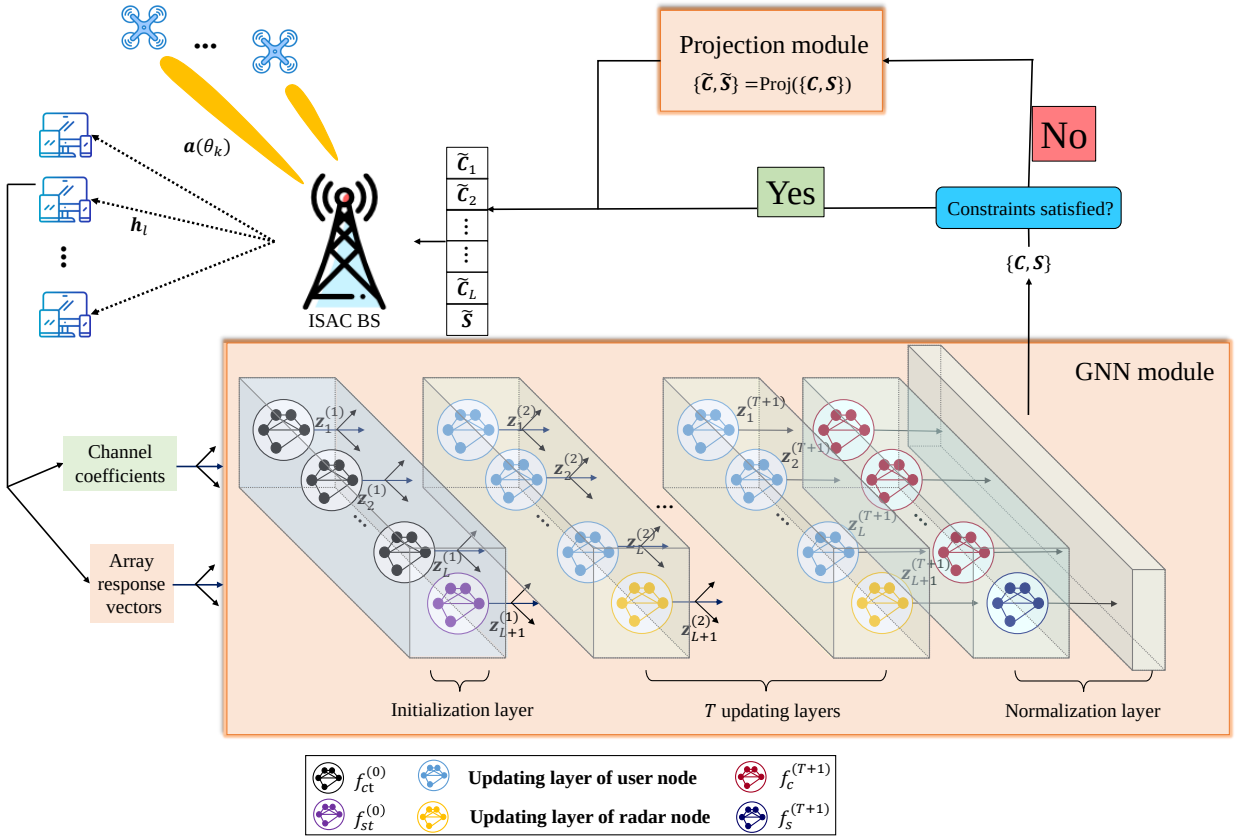

Fig. 2. Workflow of the proposed GNN-IP algorithm.

where (11c) represents the transmit power constraint and (11e) represents the communication SINR constraint. Note that we employ an equational power constraint in constraint (11c) to ensure that the maximum transmit power of the BS is utilized to maximize the radar performance [36]. Problem (11) is a high-dimensional non-convex optimization problem. Although conventional optimization-based methods (e.g., semidefinite relaxation (SDR) [37], [38]) can be utilized to solve problem (11), they usually encounter the issue of excessively high computation complexity, particularly when the numbers of sample angle grids and communication users are large, thereby lacking of algorithmic scalability.

In contrast to the optimization-based algorithms, data-driven learning algorithms can be utilized to obtain the desired beamforming matrix through direct mapping, which significantly reduces the computation complexity. However, the learning algorithm frequently encounters the critical challenge of returning infeasible solutions, especially for the communication SINR constraint (11e). Therefore, it is imperative to develop an efficient algorithm that exhibits minimal computation complexity while achieving excellent algorithmic performance in terms of scalability and constraint satisfaction. To this end, we propose a GNN-IP algorithm, where the GNN module is utilized to ensure the algorithmic scalability, and a projection module is employed to map the GNN module's output onto the feasible domain, ensuring the feasibility of the resulting beamforming matrices.

III. GNN-IP Framework

In this section, we develop a novel GNN-IP framework to maximize the sensing performance under stringent communication performance constraint. The GNN structure, loss function design, projection process, and computation complexity are elaborated in the following.

Our key idea is to learn a direct mapping from CSI and array responses to desired beamforming design, taking into account the computational efficiency and the robustness of the data-driven model training. Specifically, the general form of the mapping can be expressed as

$$\{\widetilde{\boldsymbol{C}},\widetilde{\boldsymbol{S}}\}=\mathcal{M}(\{\boldsymbol{h}_l,\boldsymbol{a}(\theta^k)\}), \tag{12}$$

where $\mathcal{M}(\cdot)$ denotes the mapping function and θ^k is the angular position for the k-th sensing target. Therefore, solving problem (11) is equivalent to acquiring the optimal mapping function $\mathcal{M}(\cdot)$. In this paper, we approximate $\mathcal{M}(\cdot)$ with the GNN-IP framework, which includes a GNN module and an implicit projection module. Since the BS knows the topology of the ISAC system, we model a graph that integrates the connectivity between BS and communication users as well as sensing targets, and construct the GNN module accordingly [39]–[41]. Specifically, the graph consists of $L+1$ nodes and $\frac{L(L+1)}{2}$ edges, where the nodes includes L user nodes, each associated with a communication vector, and one radar node associated with a combined sensing matrix. Moreover, the edges between the user nodes contain information about the

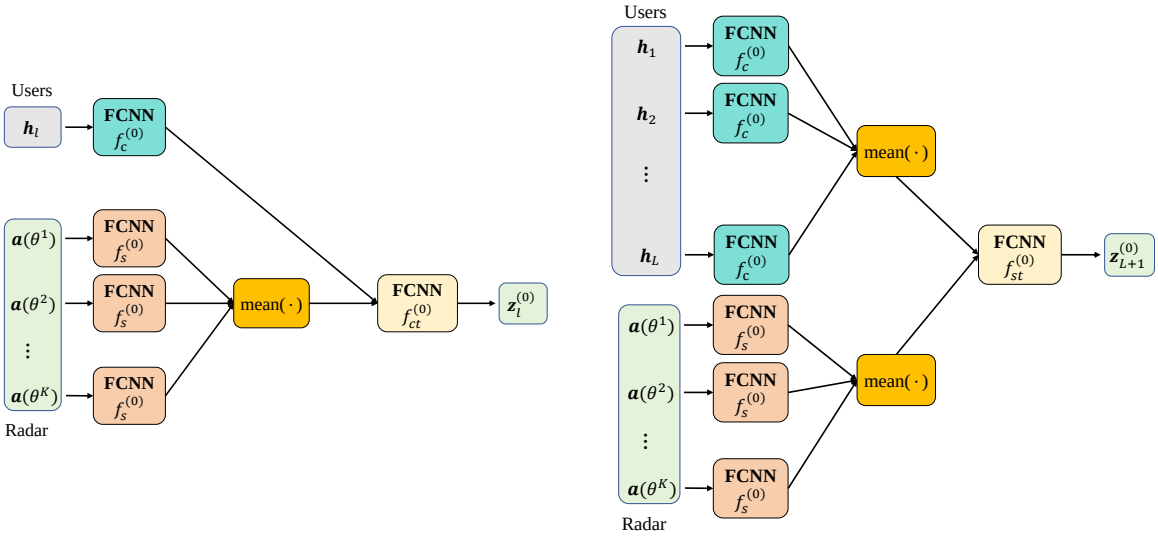

(a) User node l (b) Radar node

Fig. 3. Initialization layer for the user nodes and the radar node.

interference interaction among the communication users. The edges between the radar node and the user nodes contain two types of information. The first comprises the interference of the sensing beamforming matrix design $\boldsymbol{S}$ for communication. The second comprises the involvement of the communication beamforming matrices $\boldsymbol{C}$ for sensing. We design a unified sensing matrix instead of K individual sensing vectors due to the following two reasons. First, for power maximization towards these sensing targets, we do not need to capture the interaction among these targets, such as interference and cross-correlation. Second, the dimension of the sensing matrix $\boldsymbol{S}$ does not align with the number of sensing targets K. On the other hand, the proposed projection module employs an optimization algorithm to minimize the distance between the infeasible results generated by the GNN module and the feasible domain, ensuring the stringent constraint of problem (11). In summary, the proposed GNN-IP framework initially inputs the CSI and array responses into the GNN module, subsequently evaluating the feasibility of the GNN module output. If the output is infeasible, the projection module then maps it into the feasible domain. The overall workflow of the proposed GNN-IP framework is illustrated in Fig. 2.

A. GNN Module

The GNN module of the proposed framework consists of an initialization layer, T updating layers, and a normalization layer. Specifically, in the initialization layer, the communication channel and sensing array responses are converted into representation vectors of user nodes $\{\boldsymbol{z}_l^{(1)}\}_{l\in\mathcal{L}}$ and radar node $\boldsymbol{z}_{L+1}^{(1)}$, which are then updated via the message-passing mechanism through T updating layers, referred to as $\{\boldsymbol{z}_l^{(T+1)}\}_{l\in\mathcal{L}}$ and $\boldsymbol{z}_{L+1}^{(T+1)}$, respectively. Finally, the normalization layer maps the representation vectors to the beamforming matrices $\boldsymbol{C}$ and $\boldsymbol{S}$.

1) Initialization Layer: As shown in Fig. 3, the initialization layer separately converts the CSI of the communication users and the array responses of the sensing targets into representation vectors, facilitating message passing for the subsequent updating layers. Note that in the proposed ISAC system, it is essential that the sequence of communication beamforming designs must align with the order of communication users, while the sensing beamforming design should remains unchanged. These properties are referred to as permutation equivalence for user nodes and permutation invariance for the radar node. To realize the above two permutation properties, we separately initialize the representation vectors as follows. Specifically, the output representation vector of the l-th user node $\boldsymbol{z}_l^{(1)}$ can be represented as

$$\boldsymbol{z}_l^{(1)} = f_{ct}^{(0)}\Bigg(f_c^{(0)}\left(\left[\left(\Re\{\boldsymbol{h}_l\}\right)^{\mathrm{T}},\left(\Im\{\boldsymbol{h}_l\}\right)^{\mathrm{T}}\right]\right)^{\mathrm{T}} + \frac{1}{K}\sum_{k=1}^{K} f_s^{(0)}\left(\left[\left(\Re\{\boldsymbol{a}(\theta^k)\}\right)^{\mathrm{T}},\left(\Im\{\boldsymbol{a}(\theta^k)\}\right)^{\mathrm{T}}\right]\right)^{\mathrm{T}}\Bigg), \tag{13}$$

where $f_{ct}^{(0)}(\cdot)$, $f_c^{(0)}(\cdot)$ and $f_s^{(0)}(\cdot)$ denote the FCNN-based encoders with different sizes. Note that we consider the decomposition of the real and imaginary parts to circumvent the poor support of existing deep learning toolkits for complex numbers. Besides, as the communication beamforming matrices also participate in sensing, we incorporate the local CSI and all array responses into the initialization of representation vectors of each user node, which preserves the permutation equivalence as well.

On the other hand, we adopt a FCNN-based encoder $f_{st}^{(0)}(\cdot)$ to initialize the representation vector of the radar node. Considering the sensing beamforming matrix as interference in communication SINR calculations, the generation for representation vector of the radar node should account for the communication CSI. Therefore, the output representation vector of the radar node can be expressed as

This article has been accepted for publication in IEEE Transactions on Wireless Communications. This is the author's version which has not been fully edited and content may change prior to final publication. Citation information: DOI 10.1109/TWC.2025.3550315

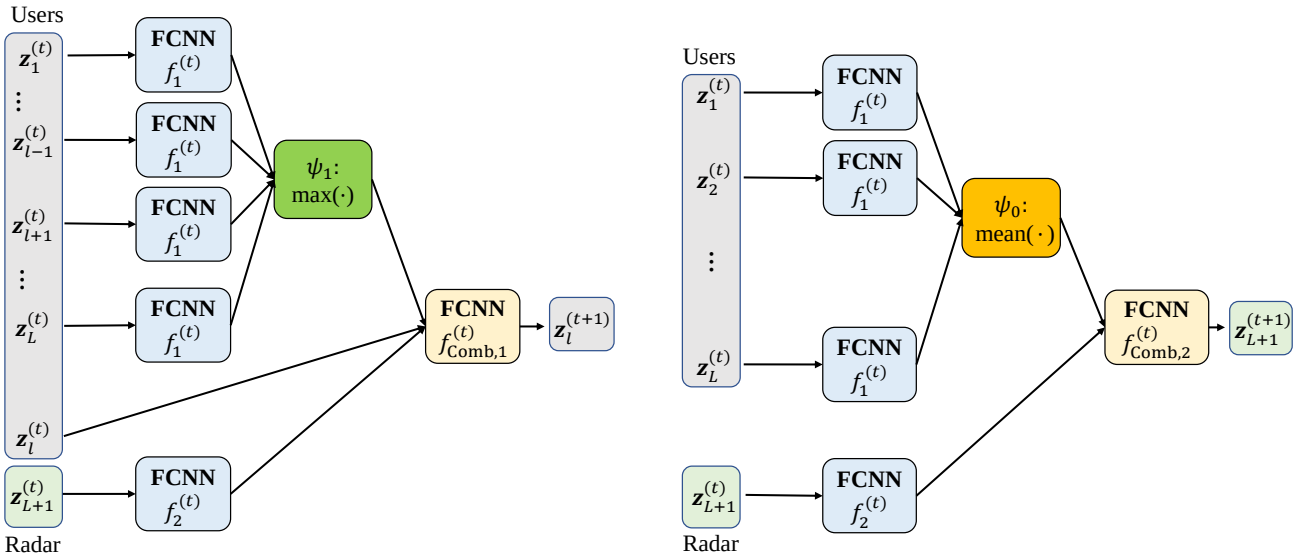

(a) User node l (b) Radar node

Fig. 4. Aggregation and combining operations of the t-th layer for the user nodes and the radar node.

$$\boldsymbol{z}_{L+1}^{(1)} = f_{st}^{(0)}\left(\frac{1}{L}\sum_{l=1}^{L} f_c^{(0)}\left([(\Re\{\boldsymbol{h}_l\})^{\mathrm{T}}, (\Im\{\boldsymbol{h}_l\})^{\mathrm{T}}]\right)^{\mathrm{T}} + \frac{1}{K}\sum_{k=1}^{K} f_s^{(0)}\left([(\Re\{\boldsymbol{a}(\theta^k)\})^{\mathrm{T}}, (\Im\{\boldsymbol{a}(\theta^k)\})^{\mathrm{T}}]\right)^{\mathrm{T}}\right), \tag{14}$$

Through the average operation, we can ensure that all the communication and sensing information are passed to the radar node, thereby ensuring the permutation invariance. In (13) and (14), we use the same encoders $f_c^{(0)}$ and $f_s^{(0)}$, thereby reducing the training complexity and ensuring the permutation properties. Besides, different encoders $f_{ct}^{(0)}$ and $f_{st}^{(0)}$ are adopted to ensure different encoding for the user and radar nodes.

2) Updating Layers: Each updating layer consists of $L+1$ nodes, each of which aggregates the representation vectors from neighboring nodes and then combines them with its own representation vector. Specifically, following the design in [40], [42]–[44], a general form of update for the representation vector at node i in the t-th updating layer can be represented as

$$\boldsymbol{v}_i^{(t+1)} = f_{\mathrm{Comb}}^{(t)}(\boldsymbol{v}_i^{(t)}, f_{\mathrm{Agg}}^{(t)}(\{\boldsymbol{v}_j^{(t)}\}_{j\in\mathcal{N}(i)})), \tag{15}$$

where $\mathcal{N}(i)$ denotes the collection of neighboring nodes of node i, and $f_{\mathrm{Comb}}^{(t)}(\cdot)$ and $f_{\mathrm{Agg}}^{(t)}(\cdot)$ denote the combining function and the aggregation function, respectively. Note that the permutation properties of the user nodes and the radar node are distinct. Consequently, the aggregation and combining operations for the user nodes and the radar node need to be designed independently.

As shown in Fig. 4(a), each user node $l \in \mathcal{L}$ aggregates the information from all other user nodes and then combines the representation vectors of local node and the radar node with the aggregated representation vectors. Specifically, the update equation for the l-th user node can be expressed as

$$\boldsymbol{z}_l^{(t+1)} = f_{\mathrm{Comb},1}^{(t)}\left(\boldsymbol{z}_l^{(t)}, f_2^{(t)}(\boldsymbol{z}_{L+1}^{(t)}),\ \boldsymbol{z}_{\mathrm{Agg},l}^{(t+1)}\right), \tag{16}$$

where

$$\boldsymbol{z}_{\mathrm{Agg},l}^{(t+1)} = \psi_1\left(\{f_1^{(t)}(\boldsymbol{z}_j^{(t)})\}_{j\in\mathcal{L}\setminus\{l\}}\right), \tag{17}$$

$f_1^{(t)}(\cdot)$ and $f_2^{(t)}(\cdot)$ are FCNN-based encoders with different sizes. $f_{\mathrm{Comb},1}^{(t)}(\cdot)$ denotes the combining function and is parameterized by a FCNN based encoder. In particular, due to the lack of theoretical guidance, we set $\psi_1(\cdot)$ as the element-wise max-pooling function, which empirically performs well, as in [26], [39], [40]. Furthermore, this choice preserves the permutation equivalence.

On the other hand, as shown in Fig. 4(b), recall that in (7) the sensing performance is jointly determined by the sensing and communication matrices, the radar node aggregates the information from all the user nodes and then combines the representation vector of local node with the aggregated representation vectors. In particular, the update equation for the radar node is represented by

$$\boldsymbol{z}_{L+1}^{(t+1)} = f_{\mathrm{Comb},2}^{(t)}\left(f_2^{(t)}(\boldsymbol{z}_{L+1}^{(t)}),\ \boldsymbol{z}_{\mathrm{Agg},L+1}^{(t+1)}\right), \tag{18}$$

where

$$\boldsymbol{z}_{\mathrm{Agg},L+1}^{(t+1)} = \psi_0\left(\{f_1^{(t)}(\boldsymbol{z}_l^{(t)})\}_{l\in\mathcal{L}}\right), \tag{19}$$

$f_{\mathrm{Comb},2}^{(t)}(\cdot)$ denotes the combining function and is parameterized by a FCNN based encoder. Besides, we adopt the element-wise mean function as $\psi_0(\cdot)$ to facilitate the integration of CSI from all users and guarantee the permutation invariance. After multiple updates, each node has access to sufficient information to coordinate between the user and radar nodes.

3) Normalization Layer: The normalization layer maps the up-to-date representation vectors to normalized beamforming matrices $\boldsymbol{C}$ and $\boldsymbol{S}$. For the representation vector $\boldsymbol{z}_l^{(T+1)}$ of the l-th user node, we first encode it through a FCNN-based encoder $f_c^{(T+1)}(\cdot)$ with the output dimension of $2M$, which can be expressed as

$$\boldsymbol{z}_l^{(T+2)} = f_c^{(T+1)}(\boldsymbol{z}_l^{(T+1)}) \in \mathbb{R}^{2M}, \forall\, l \in \mathcal{L}. \tag{20}$$

Then, we obtain the communication matrix as $\dot{\boldsymbol{C}} = [\dot{\boldsymbol{c}}_1, \ldots, \dot{\boldsymbol{c}}_L]$, where $\dot{\boldsymbol{c}}_l = \boldsymbol{z}_l^{(T+2)}(1:M) + j\boldsymbol{z}_l^{(T+2)}(M+1:2M), \forall l \in \mathcal{L}$, with $\boldsymbol{z}_l^{(T+2)}(i:j)$ being the subvector of $\boldsymbol{z}_l^{(T+2)}$ and consisting of elements i to j of $\boldsymbol{z}_l^{(T+2)}$. Similarly, for the representation vector of radar node $\boldsymbol{z}_{L+1}^{(T+1)}$, we employ the FCNN-based encoder $f_s^{(T+1)}(\cdot)$ with the output dimension of $2M^2$, and subsequently reshape it to dimension of $2M \times M$, i.e.,

$$\boldsymbol{Z}_s = \mathcal{R}\left(f_s^{(T+1)}(\boldsymbol{z}_{L+1}^{(T+1)})\right) \in \mathbb{R}^{2M \times M}, \tag{21}$$

where $\mathcal{R}(\cdot)$ denote the reshape function. Then, we obtain the sensing matrix as follows

$$\dot{\boldsymbol{S}} = \boldsymbol{Z}_s(1:M,:) + j\boldsymbol{Z}_s(M+1:2M,:), \tag{22}$$

where $\boldsymbol{Z}_s(i:j,:)$ denotes the submatrix of $\boldsymbol{Z}_s$ and consists of rows i to j of $\boldsymbol{Z}_s$. It is evident that the network output matrix inherently satisfies constraints (11b) and (11d), i.e., the positive definite and rank one conditions. Note that the randomness of neural networks may result in the violation of the transmit power constraint (11c). We propose to apply the normalization operation over the output communication matrix $\dot{\boldsymbol{C}}$ and sensing matrix $\dot{\boldsymbol{S}}$ to address this issue:

$$\begin{aligned} \boldsymbol{C} &= \frac{\sqrt{P_0}}{\mathrm{Tr}(\dot{\boldsymbol{C}}\dot{\boldsymbol{C}}^{\mathrm{H}} + \dot{\boldsymbol{S}}\dot{\boldsymbol{S}}^{\mathrm{H}})} \times \dot{\boldsymbol{C}}, \\ \boldsymbol{S} &= \frac{\sqrt{P_0}}{\mathrm{Tr}(\dot{\boldsymbol{C}}\dot{\boldsymbol{C}}^{\mathrm{H}} + \dot{\boldsymbol{S}}\dot{\boldsymbol{S}}^{\mathrm{H}})} \times \dot{\boldsymbol{S}}. \end{aligned} \tag{23}$$

Note that the normalization operation is a one-to-one mapping from the representation vectors to the beamforming matrices, thus ensuring the permutation properties of the GNN module and the satisfaction of constraint (11c).

B. Loss Function Construction

With the aforementioned design, we can transform problem (11) into an unconstrained Lagrangian problem

$$\underset{\{\boldsymbol{C}_1,\ldots,\boldsymbol{C}_L,\boldsymbol{S}\}}{\text{minimize}} \; L(\boldsymbol{R}) + \lambda \sum_{l=1}^{L} (\Gamma_0 - \Gamma_l), \tag{24}$$

where $\boldsymbol{C}_l = \boldsymbol{c}_l\boldsymbol{c}_l^{\mathrm{H}}$ and $\boldsymbol{R} = \sum_{l=1}^{L}\boldsymbol{C}_l + \boldsymbol{S}\boldsymbol{S}^{\mathrm{H}}$, and λ is the Lagrangian dual variable. Inspired by the objective plus penalty structure in (24), we propose to design the loss function as follows

$$\text{loss} = \underbrace{L(\boldsymbol{R})}_{t_1} + \mu \underbrace{\sum_{l=1}^{L} \mathcal{K}\left(\Gamma_0 - \Gamma_l\right)}_{t_2}, \tag{25}$$

where $\mathcal{K}(\cdot)$ denotes the barrier function and μ is a hyper-parameter associated with constraint (11c). In this paper, we adopt the ReLU function as the barrier function due to its low computation complexity and ease of optimization. The barrier function enables the loss function to prioritize sensing performance while incorporating communication SINR constraint.

The proposed GNN module has the following advantages. First, our proposed GNN module is capable of preserving permutation invariance and permutation equivalence of problem (11). The GNN module consistently generates the same permutation order for communication beamforming vectors $\boldsymbol{c}_l$ and the invariant sensing beamforming matrix $\boldsymbol{S}$ when the communication users in the system are permuted. Specifically, permutation equivalence means that when we arrange the communication users in the system, the GNN module produces the communication beam forming vectors $\boldsymbol{c}_l$ with the same order of arrangement, whereas permutation invariance means that the arrangement of the communication users does not change the sensing beam forming matrix $\boldsymbol{S}$ as well as the covariance matrix $\boldsymbol{R} = \sum_{l=1}^{L}\boldsymbol{C}_l + \boldsymbol{S}\boldsymbol{S}^{\mathrm{H}}$. The permutation properties can improve the scalability of the learning framework. Second, compared to the conventional FCNNs, the GNN module leverages the network topology to capture the interaction between communication users and sensing targets. This not only helps mitigate co-channel interference for communication users, but also significantly enhances the sensing performance. Third, the user nodes of the proposed GNN module share the same design of encoder and decoder. This design allows us to directly and easily copy or delete user nodes without retraining when the number of communication users changes, which reduces the computation time and enhances the scalability of the algorithm. Additionally, benefiting from data-driven training and sufficient exploration over the graph for the considered ISAC system, the learned GNN module can capture the general representation of the ISAC system with respect to channel state information and array responses, and is robust to the randomness of fading channel and location changes of sensing targets, thereby reducing the number of retraining. In summary, the proposed GNN module exhibits the characteristics of low complexity, high training efficiency, and high algorithmic scalability.

The proposed GNN module effectively reduces computation complexity while enhancing the sensing performance and mitigating the communication constraints violation. Nevertheless, the stringent transmit power and communication SINR constraints may not always be satisfied. To ensure robustness, we propose a projection module to post-process the output of the GNN module in the following subsection.

C. Implicit Projection Module

After the pre-processing via the GNN module, we post-process the outputs of the GNN module that violate constraint (11c) by developing an implicit projection module. By denoting the projection function as $\mathrm{Proj}(\cdot)$, the desired communication beamforming and sensing beamforming matrices can be expressed as

$$\{\widetilde{\boldsymbol{C}}, \widetilde{\boldsymbol{S}}\} = \mathrm{Proj}\left(\{\boldsymbol{C}, \boldsymbol{S}\}\right). \tag{26}$$

As illustrated in Fig. 5, we adopt the implicit projection method to project beamforming matrices $\{\boldsymbol{C}, \boldsymbol{S}\}$ generated by the GNN module into the feasible domain [45], [46]. Specifically, we formulate the following projection optimiza-

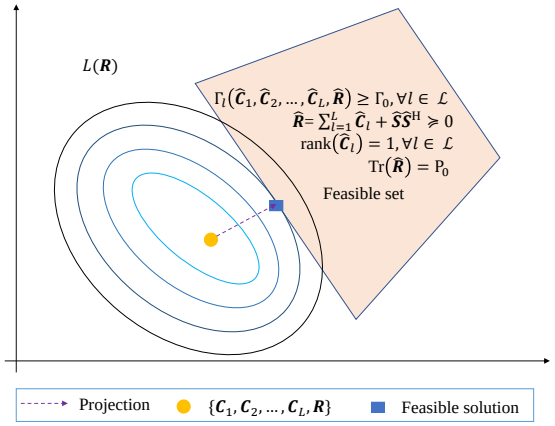

Fig. 5. Illustration of the proposed projection module, where the round point represents the output of the GNN module and is projected into the feasible domain, denoted as the square point, via the projection module.

tion problem

$$\underset{\hat{\boldsymbol{C}}_1,\ldots,\hat{\boldsymbol{C}}_L,\hat{\boldsymbol{R}}}{\text{minimize}} \quad \mathcal{D}\left(\{\hat{\boldsymbol{C}}_1,\ldots,\hat{\boldsymbol{C}}_L,\hat{\boldsymbol{R}}\},\{\boldsymbol{C}_1,\ldots,\boldsymbol{C}_L,\boldsymbol{R}\}\right) \tag{27a}$$

$$\text{subject to } \hat{\boldsymbol{R}} \succeq 0, \tag{27b}$$

$$\hat{\boldsymbol{R}} - \left(\sum_{l=1}^{L} \hat{\boldsymbol{C}}_l\right) \succeq 0, \tag{27c}$$

$$\mathrm{Tr}(\hat{\boldsymbol{R}}) = P_0, \tag{27d}$$

$$\Gamma_l \geq \Gamma_0, \forall\, l \in \mathcal{L}, \tag{27e}$$

where $\mathcal{D}(\cdot)$ denotes the function that measures the distance between the output beamforming designs of the GNN module and the desired designs in the feasible domain. By setting $\mathcal{D}(\cdot)$ as the Frobenius norm, problem (27) can be rewritten as

$$\underset{\hat{\boldsymbol{C}}_1,\ldots,\hat{\boldsymbol{C}}_L,\hat{\boldsymbol{R}}}{\text{minimize}} \quad \sum_{l=1}^{L} \|\hat{\boldsymbol{C}}_l - \boldsymbol{C}_l\|_{\mathrm{F}}^2 + \|\hat{\boldsymbol{R}} - \boldsymbol{R}\|_{\mathrm{F}}^2 \tag{28a}$$

$$\text{subject to } \hat{\boldsymbol{R}} \succeq 0, \tag{28b}$$

$$\hat{\boldsymbol{R}} - \left(\sum_{l=1}^{L} \hat{\boldsymbol{C}}_l\right) \succeq 0, \tag{28c}$$

$$\mathrm{Tr}(\hat{\boldsymbol{R}}) = P_0, \tag{28d}$$

$$\Gamma_l \geq \Gamma_0, \forall\, l \in \mathcal{L}. \tag{28e}$$

Based on (9), we reformulate (28e) and obtain the following convex optimization problem

$$\underset{\hat{\boldsymbol{C}}_1,\ldots,\hat{\boldsymbol{C}}_L,\hat{\boldsymbol{R}}}{\text{minimize}} \quad \sum_{l=1}^{L} \|\hat{\boldsymbol{C}}_l - \boldsymbol{C}_l\|_{\mathrm{F}}^2 + \|\hat{\boldsymbol{R}} - \boldsymbol{R}\|_{\mathrm{F}}^2 \tag{29a}$$

$$\text{subject to } \hat{\boldsymbol{R}} \succeq 0, \tag{29b}$$

$$\hat{\boldsymbol{R}} - \left(\sum_{l=1}^{L} \hat{\boldsymbol{C}}_l\right) \succeq 0, \tag{29c}$$

$$\mathrm{Tr}(\hat{\boldsymbol{R}}) = P_0, \tag{29d}$$

$$(1 + \Gamma_0^{-1})\boldsymbol{h}_l^{\mathrm{H}} \hat{\boldsymbol{C}}_l \boldsymbol{h}_l \geq \boldsymbol{h}_l^{\mathrm{H}} \hat{\boldsymbol{R}} \boldsymbol{h}_l + \sigma^2, \forall\, l \in \mathcal{L}. \tag{29e}$$

Note that the constraints of problems (29) and (11) are equivalent except for the rank-one constraint (11d). To satisfy the rank-one constraint, the communication beamforming vectors $\{\widetilde{\boldsymbol{c}}_1, \ldots, \widetilde{\boldsymbol{c}}_L\}$ can be explicitly expressed as

$$\widetilde{\boldsymbol{c}}_l = \frac{\hat{\boldsymbol{C}}_l \boldsymbol{h}_l}{\sqrt{\boldsymbol{h}_l^{\mathrm{H}} \hat{\boldsymbol{C}}_l \boldsymbol{h}_l}}, \forall\, l \in \mathcal{L}, \tag{30}$$

and the explicit expression of sensing beamforming matrix $\widetilde{\boldsymbol{S}}$ can be obtained after applying the Cholesky decomposition as follows

$$\widetilde{\boldsymbol{S}}\widetilde{\boldsymbol{S}}^{\mathrm{H}} = \hat{\boldsymbol{R}} - \left(\sum_{l=1}^{L} \widetilde{\boldsymbol{C}}_l\right), \tag{31}$$

where $\widetilde{\boldsymbol{C}}_l = \widetilde{\boldsymbol{c}}_l \widetilde{\boldsymbol{c}}_l^{\mathrm{H}}$. Then, we need to prove that set $\{\widetilde{\boldsymbol{c}}_1, \ldots, \widetilde{\boldsymbol{c}}_L, \widetilde{\boldsymbol{S}}\}$ complies with the constraints in problem (29) to validate its feasibility as a solution set for problem (11).

Proposition 1. *The set* $\{\widetilde{\boldsymbol{c}}_1, \ldots, \widetilde{\boldsymbol{c}}_L, \widetilde{\boldsymbol{S}}\}$ *obtained by* (30) *and* (31) *satisfies the constraints in problem (*29*).*

Proof. With (30) and (31), as $\boldsymbol{h}_l^{\mathrm{H}} \widetilde{\boldsymbol{C}}_l \boldsymbol{h}_l = \boldsymbol{h}_l^{\mathrm{H}} \hat{\boldsymbol{C}}_l \boldsymbol{h}_l$, the obtained $\widetilde{\boldsymbol{C}}_l$ satisfies the communication SINR constraint (29e). Since $\hat{\boldsymbol{R}} - \left(\sum_{l=1}^{L} \hat{\boldsymbol{C}}_l\right) \succeq 0$, we can apply the Cauchy-Schwartz inequality, for any $\boldsymbol{u}$ and $\forall\, l \in \mathcal{L}$, leading to

$$\boldsymbol{u}^{\mathrm{H}}(\hat{\boldsymbol{C}}_l - \widetilde{\boldsymbol{C}}_l)\boldsymbol{u} = \boldsymbol{u}^{\mathrm{H}} \hat{\boldsymbol{C}}_l \boldsymbol{u} - (\boldsymbol{h}^{\mathrm{H}} \widetilde{\boldsymbol{C}}_l \boldsymbol{h}_l)^{-1} \left|\boldsymbol{u}^{\mathrm{H}} \widetilde{\boldsymbol{C}}_l \boldsymbol{h}_l\right|^2 \geq 0, \tag{32}$$

which means that $\hat{\boldsymbol{C}}_l - \widetilde{\boldsymbol{C}}_l \succeq 0, \forall\, l \in \mathcal{L}$. Therefore, we obtain

$$\hat{\boldsymbol{R}} - \left(\sum_{l=1}^{L} \widetilde{\boldsymbol{C}}_l\right) = \hat{\boldsymbol{R}} - \left(\sum_{l=1}^{L} \hat{\boldsymbol{C}}_l\right) + \sum_{l=1}^{L} (\hat{\boldsymbol{C}}_l - \widetilde{\boldsymbol{C}}_l) \succeq 0. \tag{33}$$

With the derivation above, it is verified that $\{\widetilde{\boldsymbol{C}}_l\}_{l \in \mathcal{L}}$ along with $\widetilde{\boldsymbol{S}}$ constitute a feasible solution to problem (29). □

The entire process of the proposed GNN-IP algorithm is summarized in **Algorithm 1**. The proposed algorithm has the following advantages. First, the computation complexity of problem (11) depends on the sample grid number N, whereas that of problem (29) is independent of N. Consequently, for a large value of N, the projection module requires a lower computation complexity than problem (11). Besides, as shown in (23) and (25), the proposed GNN module incorporates constraints in the normalization layer and loss function design. Consequently, only a few infeasible samples enter the projection module, thereby significantly reducing the algorithmic complexity. Second, the proposed GNN-IP framework guarantees permutation equivalence/invariance, while ensuring that the generated solutions are feasible.

D. Computation Complexity

1) Complexity of GNN-IP Algorithm: As the proposed GNN-IP framework consists of the GNN module and the projection module, we analyze the complexity of these two modules separately.

Algorithm 1 Joint Transmit Beamforming via GNN-IP algorithm.

Input:
BS transmit power P_0;
SINR threshold Γ_0.
Training dataset
$\mathcal{D} = \{\{\boldsymbol{h}_l, \boldsymbol{a}(\theta^k)\}_{(1)}, \ldots, \{\boldsymbol{h}_l, \boldsymbol{a}(\theta^k)\}_{(D_{train})}\}$;
Test dataset
$\mathcal{T} = \{\{\boldsymbol{h}_l, \boldsymbol{a}(\theta^k)\}_{(1)}, \ldots, \{\boldsymbol{h}_l, \boldsymbol{a}(\theta^k)\}_{(D_{test})}\}$;
Initial GNN model $\mathcal{G}$.
Output:
Transmit beamforming matrices $\{\widetilde{\boldsymbol{c}}_1, \ldots, \widetilde{\boldsymbol{c}}_L, \widetilde{\boldsymbol{S}}\}$.
Steps:
$Training$:
while Training **do**
  for $i = 0$ to D_{train} **do**
    Sample $\{\boldsymbol{h}_l, \boldsymbol{a}(\theta^k)\}_{(i)}$ from $\mathcal{D}$;
    for $l = 0$ to L **do**
      Obtain representation vector $\boldsymbol{z}_l^{(0)}$ based on (13);
    end for
    Obtain representation vector $\boldsymbol{z}_{L+1}^{(0)}$ based on (14);
    for $t = 0$ to T **do**
      for $l = 0$ to L **do**
        Update representation vector $\boldsymbol{z}_l^{(t)}$ based on (17);
      end for
      Update representation vector $\boldsymbol{z}_{L+1}^{(t)}$ based on (18);
    end for
    Obtain network output matrices $\boldsymbol{C}$ and $\boldsymbol{R}$ based on (23);
    Calculate loss based on (25);
    Update GNN $\mathcal{G}$ model with gradient backward;
  end for
end while
$Inference$:
for $i = 0$ to D_{test} **do**
  Sample $\{\boldsymbol{h}_l, \boldsymbol{a}(\theta^k)\}_{(i)}$ from $\mathcal{T}$;
  Obtain transmit beamforming matrices $\{\boldsymbol{C}, \boldsymbol{R}\}$ through the GNN inference;
  if $\boldsymbol{C}, \boldsymbol{R}$ is infeasible **then**
    Project the solution to the feasible domain based on (29);
    Compute $\{\widetilde{\boldsymbol{c}}_1, \ldots, \widetilde{\boldsymbol{c}}_L, \widetilde{\boldsymbol{S}}\}$ based on (30) and (31).
  else
    Output $\{\widetilde{\boldsymbol{c}}_1, \ldots, \widetilde{\boldsymbol{c}}_L, \widetilde{\boldsymbol{S}}\}$ based on $\{\boldsymbol{C}, \boldsymbol{R}\}$.
  end if
end for

a) Complexity of GNN Module: Since the encoders share the same structure in different layers, we assume that the encoders of the user and the radar node have the same network structure with different weights, and denote the computation complexity of them as $\mathcal{O}(C)$. For the initialization layer, since each node takes into account the CSI of L communication users and the array responses of K sensing targets when generating the representation vector, the computation complexity is $\mathcal{O}(CL(K+1) + C(L+K)) = \mathcal{O}(C(LK+2L+K)$. For the updating layer, each node performs the aggregation and combining operations. For the user node, according to (17), the computation complexity of encoding and max pooling in aggregation operations is $\mathcal{O}(CL+L-1)$. For the sensing node, according to (18), the computation complexity of encoding and mean function in aggregation operations is $\mathcal{O}(CL + L)$. Since the combining functions share the same structure in all nodes, we assume that the combining operation takes the same amount of time for all nodes, denoted as $\mathcal{O}(C)$. Therefore, the computation complexity of T updating layers is $\mathcal{O}(TL(CL + L + C))$. For the normalization layer, the computation complexity is $\mathcal{O}(C(L + 1))$. As a result, the overall computation complexity of the GNN module in the inference stage is $\mathcal{O}(C(LK+2L+K)+TL(CL+L+C)+C(L+1)) \approx \mathcal{O}(C(TL^2+TL+KL+L+K))$.

b) Computation Complexity of Projection Module: Solving problem (29) is the most time-consuming procedure of the projection module. Specifically, the CVX toolbox transforms problem (29) into a second-order cone programming (SOCP) problem during the solving stage, where (29a) is transformed into L constraints [47]. Hence the worst-case computation complexity to solve problem (29) is $\mathcal{O}(\max(L, LM)^4(LM)^{0.5}\log(\frac{1}{\epsilon})) = \mathcal{O}((LM)^{4.5}\log(\frac{1}{\epsilon}))$, given a solution accuracy ϵ [38].

We assume that the ratio of the number of samples that satisfy the constraints to the total number of samples after the inference of the GNN module is ρ. The computation complexity of the whole GNN-IP algorithm is $\mathcal{O}(\rho(C(TL^2+TL+KL+L+K)) + (1-\rho)((LM)^{4.5}\log(\frac{1}{\epsilon})))$. Hence, the primary factors influencing the computation complexity include the ratio of constraint satisfaction, the number of communication users and sensing targets, and the number of antennas.

2) Computation Complexity of SDR Algorithm: According to [33], we first transform problem (11) into a semi-definite programming (SDP) problem, which is then transformed into a SOCP problem during the solving stage, where (11a) is transformed into N constraints. Given a solution accuracy ϵ, the worst-case computation complexity to solve (11) using the SDR algorithm is $\mathcal{O}(\max(N, LM)^4(LM)^{0.5}\log(\frac{1}{\epsilon}))$ [38]. Hence, the computation complexity of the SDR algorithm is always greater than or equal to that of the developed projection module. In particular, to enhance the sensing performance, the value of N should be large. When $N > LM$, the projection module results in lower computation complexity than the SDR algorithm. By further considering that the projection model is infrequently used, the worst-case computation complexity of the proposed algorithm is much smaller than that of the SDR algorithm.

IV. Simulation Results

In this section, we evaluate the performance of our proposed GNN-IP algorithm for ISAC through extensive simulations.

A. System Settings

In the simulations, the BS is equipped with $M = 10$ antennas, and located at $(x, y, z) = (0, -100, 20)$ meters. The

TABLE I
NETWORK PARAMETERS OF THE PROPOSED GNN MODULE.

Name	Size	Activation Function
$f_c^{(0)}, f_s^{(0)}$	$2M \times 128 \times 128$	Sigmoid
$f_{ct}^{(0)}, f_{st}^{(0)}$	$128 \times 128 \times 128$	Sigmoid
$f_1^{(1)}, f_2^{(1)}$	$128 \times 64 \times 128$	Sigmoid
$f_{\text{Comb},1}^{(1)}$	$128 \times 64 \times 128$	Sigmoid
$f_{\text{Comb},2}^{(1)}$	$128 \times 64 \times 128$	Sigmoid
$f_1^{(2)}, f_2^{(2)}$	$128 \times 64 \times 128$	Sigmoid
$f_{\text{Comb},1}^{(2)}$	$128 \times 64 \times 128$	Sigmoid
$f_{\text{Comb},2}^{(2)}$	$128 \times 64 \times 128$	Sigmoid
$f_c^{(3)}$	$128 \times 2M$	None
$f_s^{(3)}$	$128 \times 2M^2$	None

BS simultaneously serves three radar targets and two communication users, i.e., $K = 3$ and $L = 2$. The transmit power of the BS is normalized to $P_0 = 1$. The communication users are independent and identically distributed within a rectangular region of $([5, 35], [-35, 35], 0)$ meters. The channel between the BS and user l is modeled as Rayleigh fading, i.e., $\boldsymbol{h}_l = \sqrt{\alpha_l}\boldsymbol{h}_l^*$, where $\boldsymbol{h}_l^* \sim \mathcal{CN}(\boldsymbol{0}, \boldsymbol{I})$. The factor α_l, representing the large-scale fading, is modeled as $\alpha_l = 10^{-3} d_l^{-2.67}$, where d_l represents the distance between the BS and user l. The width of each sensing beam is $\Delta = 10^\circ$, and thus the desired beampattern $b(\theta)$ is set as

$$b(\theta) = \begin{cases} 1, \hat{\theta}_p - \frac{\Delta}{2} \le \theta \le \hat{\theta}_p + \frac{\Delta}{2}, p = 1, 2, 3, \\ 0, \text{otherwise}. \end{cases} \tag{34}$$

For (7), we uniformly sample the direction grids $\{\theta_n\}_{n=1}^N$ within the range of -90° to 90° with a resolution of 1°, i.e., $N = 180$. Unless specified otherwise, we set $\sigma^2 = 10^{-10}$ and $\Gamma_0 = 8$ dB.

B. Network Parameters and Benchmarks

We consider a 2-layer GNN and the specific parameters of the FCNN in each graph layer are shown in Table I. For the power normalization parameter β in (7), we obtain its value by solving the linear equation problem $\beta \boldsymbol{b} = \boldsymbol{p}$, where $\boldsymbol{b} = [b(\theta_1), b(\theta_2), \ldots, b(\theta_N)]^{\mathrm{T}}$ and $\boldsymbol{p} = [P(\theta_1; \boldsymbol{R}), P(\theta_2; \boldsymbol{R}), \ldots, P(\theta_N; \boldsymbol{R})]^{\mathrm{T}}$.

Our proposed neural network is implemented by the PyTorch deep learning library [48]. We employ the Adam optimizer [49] with a learning rate of 7×10^{-3} for the network training. We consider a total of 500 training epochs, and perform validation and test after every 10 training epochs. The model with the best performance on the validation set is saved. The sizes of the training, validation, and test sets are fixed as 10000, 1000, and 1000, respectively. In each simulation, once the number of communication users and SINR constraints of the system are fixed, the proposed GNN-IP algorithm directly inference on the changing communication channel and array responses without retraining.

We consider the following benchmarks:

- *Benchmark 1* is the SDR based optimization algorithm proposed in [33].
- *Benchmark 2* is the zero-forcing (ZF) beamforming based optimization algorithm proposed in [33]. ZF-beamforming is utilized to reduce inter-user interference and radar interference, which in turn accelerates the algorithm convergence to obtain a sub-optimal solution.
- *Benchmark 3* is the deep neural network (DNN) based algorithm. We design a conventional FCNN for comparison. Specifically, we employ a DNN comprising four fully-connected layers, with each hidden layer comprising 512 neurons. We employ the sigmoid function as the activation function. The proposed network is implemented using PyTorch, and we utilize the Adam optimizer with a learning rate of 10^{-3} for neural network training. The sizes of the training, validation, and test sets are the same as that of the proposed GNN module. We consider a total of 500 training epochs, and perform validation and test after every 10 training epochs. The model with the best performance on the validation set is saved. We employ the normalization operation described in (23) and use (25) as the loss function for network training.

We implement the optimization-based benchmark algorithms via the MATLAB CVX toolbox [47], [50] with the SDPT3 solver [51]. The results are obtained by averaging over 1000 Monte Carlo tests.

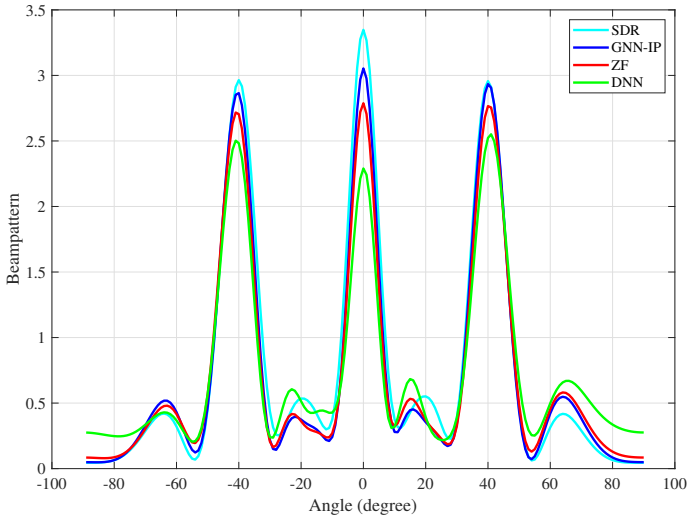

Fig. 6. Transmit beampattern of MIMO radar when $\hat{\theta}_1 = -40^\circ$, $\hat{\theta}_2 = 0^\circ$, and $\hat{\theta}_3 = 40^\circ$.

C. Performance Comparison

1) Beampattern: We depict the beampattern $P(\theta; \boldsymbol{R})$ in Fig. 6 and Fig. 7, where we set the number of communication users $L = 2$. We train and compute the beampatterns for two scenarios with directions $\{\hat{\theta}_1, \hat{\theta}_2, \hat{\theta}_3\}$ as $\{-40^\circ, 0^\circ, 40^\circ\}$ and $\{-40^\circ, 15^\circ, 30^\circ\}$. We observe that the proposed GNN-IP algorithm maintains accurate angle sensing of the target direction. Our algorithm demonstrates superior beampattern performance at the target angle compared to ZF and DNN, closely approaching the performance of SDR. Meanwhile, the proposed algorithm has excellent sensing performance even

This article has been accepted for publication in IEEE Transactions on Wireless Communications. This is the author's version which has not been fully edited and content may change prior to final publication. Citation information: DOI 10.1109/TWC.2025.3550315

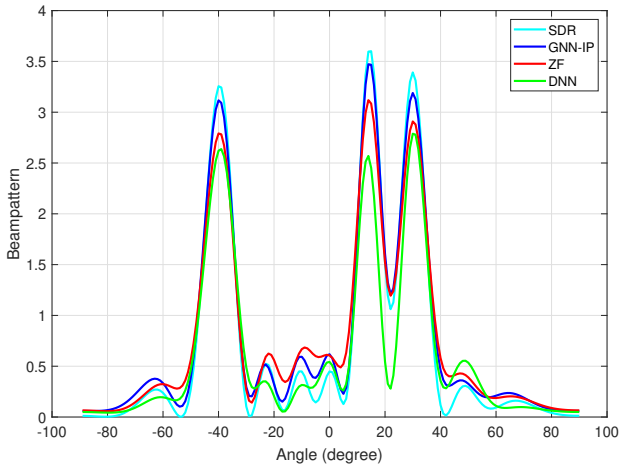

Fig. 7. Transmit beampattern of MIMO radar when $\hat{\theta}_1 = -40°$, $\hat{\theta}_2 = 15°$, and $\hat{\theta}_3 = 30°$.

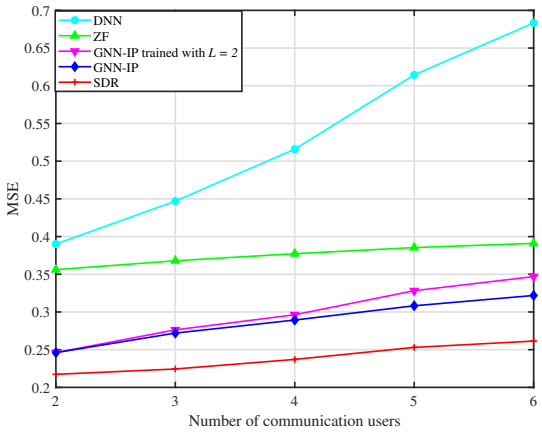

Fig. 9. Beampattern MSE versus number of communication users.

when the sensing targets are close in directions. Moreover, due to the full rank sensing beamforming design $\boldsymbol{S}$, we successfully sense every target even though the number of communication users is smaller than the number of sensing targets.

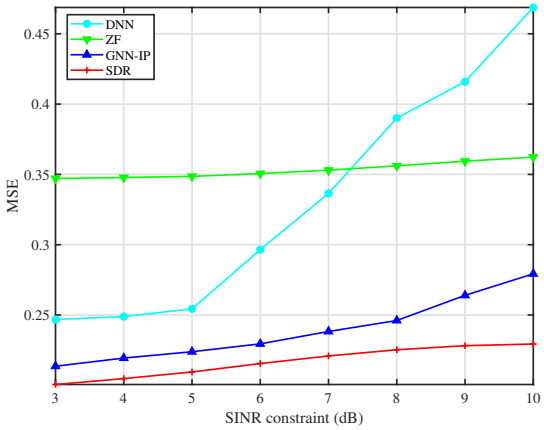

Fig. 8. Beampattern MSE versus SINR threshold Γ_0 in a dynamic scenario.

2) MSE: We then evaluate the sensing MSE performance of different algorithms versus the communication SINR constraint Γ_0 in Fig. 8, and versus the number of communication users L in Fig. 9. In Fig. 8, we evaluate the sensing MSE performance of the proposed algorithm and the baseline algorithms in a dynamic scenario. Specifically, after each time slot, every communication user randomly moves within $[-1, 1]$ meter along the x-axis and $[-2, 2]$ meters along the y-axis from its current position. In each time slot, the proposed algorithm as well as the baseline algorithms are executed to optimize the resource allocation. Fig. 8 shows that the proposed GNN-IP algorithm achieves better sensing performance than the DNN algorithm and ZF optimization algorithm. Meanwhile, the performance gap between the GNN-IP algorithm and the SDR algorithm is small when $\Gamma_0 \leq 8$ dB. As Γ_0 increases to 9 dB, the GNN-IP algorithm needs to leverage the projection module to ensure the solution feasibility, leading to a degradation of its sensing performance and a relatively large performance loss compared to the SDR algorithm. This illustrates the feasibility of the proposed algorithm in dynamic scenarios.

Fig. 9 also indicates that the proposed GNN-IP algorithm can achieve a satisfactory performance under different values of L. To illustrate the scalability of the proposed algorithm, we train a GNN module on the dataset with $L = 2$, and then directly apply it to a multi-user scenario. Benefiting from the shared encoder and decoder design of the user nodes, the proposed algorithm adapts to different user number scenarios by directly copying the network weight information of the encoders of the user nodes of the GNN module without retraining. From Fig. 9, we find that the performance of the scaled GNN-IP algorithm is close to that of the GNN-IP algorithm that performs retraining until the number of users reaches 4. This illustrates the scalability of the proposed GNN algorithm.

3) Computation Complexity: Despite achieving a little higher MSE than the SDR algorithm, the proposed GNN-IP algorithm has much lower computation complexity. To verify this, Table II and Table III compare the average computation time and the sensing MSE of our proposed algorithm with that of the SDR algorithm and the ZF algorithm under different number of sample grids N and different communication SINR constraints, respectively.

From Table II, we observe that the computation time of the conventional optimization algorithm rapidly increases with the increase of N. However, with any value of N, the computation time of the proposed GNN-IP algorithm remains almost unchanged and is much smaller than that of the traditional optimization-based algorithms. This is due to the fact that the network mapping of the GNN module and the computation complexity of the projection module are independent of N. This demonstrates the low computation complexity of our proposed GNN-IP algorithm compared to traditional optimization-based algorithms. Meanwhile, it can be observed that the sensing MSE for all algorithms increases rapidly as N decreases. It is evident that under limited computation time, our proposed GNN-IP algorithm is able to use a larger N

TABLE II
A COMPARISON OF OUR PROPOSED GNN-IP ALGORITHM, ZF ALGORITHM AND SDR ALGORITHM IN TERMS OF AVERAGE COMPUTATION TIME AND SENSING MSE WITH DIFFERENT NUMBER OF SAMPLE GRIDS N.

	GNN − IP		**ZF**		**SDR**	
Number of sample grids N	MSE	Time (s)	MSE	Time (s)	MSE	Time (s)
180	0.2461	0.0002	0.3561	4.8713	0.2253	6.9714
60	0.2515	0.0002	0.3652	1.7279	0.2446	2.0613
30	0.3418	0.0002	0.7235	0.7234	0.3797	0.9849
10	0.9332	0.0002	1.1150	0.6647	1.2050	0.5741

TABLE III
A COMPARISON OF OUR PROPOSED GNN-IP ALGORITHM, ZF ALGORITHM AND SDR ALGORITHM IN TERMS OF AVERAGE COMPUTATION TIME AND SENSING MSE WITH DIFFERENT COMMUNICATION SINR CONSTRAINTS Γ_0.

	GNN − IP				**ZF**		**SDR**	
Γ_0 (dB)	MSE	GNN module time (s)	Projection module time (s) and usage (%)	GNN-IP algorithm time (s)	MSE	Time (s)	MSE	Time (s)
3	0.2136	0.0002	0 (0%)	0.0002	0.3471	4.7716	0.2006	6.9182
4	0.2194	0.0002	0 (0%)	0.0002	0.3478	4.8177	0.2048	6.7799
5	0.2239	0.0002	0 (0%)	0.0002	0.3486	4.7980	0.2095	6.7848
6	0.2295	0.0002	0 (0%)	0.0002	0.3506	4.8229	0.2155	6.8487
7	0.2383	0.0002	0 (0%)	0.0002	0.3530	4.7728	0.2209	6.7185
8	0.2461	0.0002	0 (0%)	0.0002	0.3561	4.8713	0.2253	6.9714
9	0.2640	0.0002	0.0485 (3.2%)	0.0233	0.3594	4.7793	0.2282	7.0134
10	0.2793	0.0002	0.0525 (7.6%)	0.0873	0.3623	4.9473	0.2294	7.0597

than the conventional optimization-based methods, to achieve desired sensing performance.

Table III also shows the average ratio of the projection module being used and the corresponding average computation time during the inference stage. From Table III, it can be clearly observed that our proposed GNN-IP algorithm enjoys a significantly lower inference computation complexity than the SDR and ZF algorithms under various SINR constraints. We also find that the computation time of the GNN-IP algorithm increases as the communication SINR constraint increases. This arises from the inclusion of the projection module in the GNN-IP algorithm to meet stringent communication performance requirements. Nevertheless, it can be observed that when the communication SINR threshold $\Gamma_0 \leq 8$, the projection module is not used, and the computation time of the projection module is 0. When $\Gamma_0 \geq 9$, the output of the GNN module may not always be feasible, and hence the projection module is employed to ensure that the constraints are satisfied. However, the projection module is not frequently used and the computation time of our proposed algorithm is still much smaller than that of the SDR algorithm. We also observe that the proposed GNN-IP algorithm outperforms the ZF algorithm in terms of both the algorithmic performance and the computational complexity. It is worth noting that when the communication SINR constraints change, the proposed GNN-IP algorithm needs to be retrained. However, the system settings do not change as frequently as the communication channel state information. The proposed GNN-IP algorithm exhibits low computation complexity and can be applied in many practical scenarios, such as smart agriculture, video streaming, environment monitoring, and remote control automation [52].

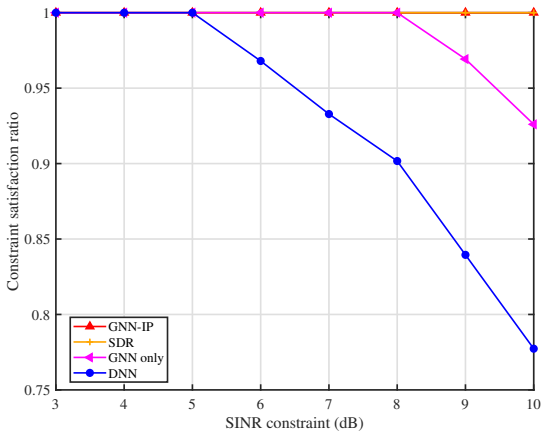

Fig. 10. Satisfaction ratio versus SINR threshold Γ_0

4) Constraint Satisfaction Ratio: In Fig. 10 and Fig. 11, we investigate the satisfaction ratio of different algorithms under different communication SINR constraints and different number of communication users, where the GNN only algorithm denotes our proposed GNN-IP algorithm without the projection module. We denote the satisfaction ratio as the ratio of the number of samples where the solution feasibility holds to the total number of samples. We can conclude from Fig. 10 that the satisfaction ratios of the GNN only algorithm and the DNN algorithm decrease as the communication SINR

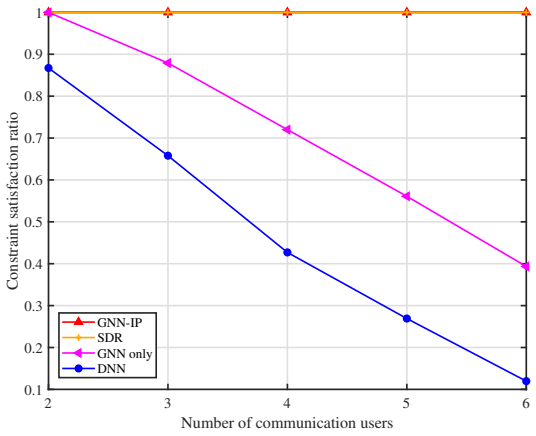

Fig. 11. Satisfaction ratio versus number of communication users.

constraint becomes more stringent. Although some efforts, including adding normalization layer and introducing penalty terms in the loss function, have been put forward, neither the GNN only algorithm nor the DNN algorithm guarantees the feasibility of solutions when the communication performance is highly demanding. Besides, the GNN only algorithm exhibits a slower decline in satisfaction ratio compared to the DNN algorithm, which demonstrates the superiority of the graph structure design of our proposed GNN only algorithm. In contrast, the satisfaction ratio of the GNN-IP algorithm remains 100% for all values of Γ_0 in Fig. 10, since the projection module in the GNN-IP algorithm can strictly guarantee the solution feasibility. When the communication SINR constraint Γ_0 increases to 9 dB, the satisfaction ratio achieved by the GNN only algorithm starts to decline, signifying the activation of the projection module in the proposed GNN-IP algorithm. This coincides with the observation that the algorithmic performance and the computation time of the proposed GNN-IP algorithm deteriorate at $\Gamma_0 = 9$ dB, as shown in Fig. 8 and Table III. From Fig. 11, we also observe that the satisfaction ratios of both the GNN only algorithm and the DNN algorithm decrease with the increase of the user number. In contrast, the proposed GNN-IP algorithm consistently maintains a 100% satisfaction ratio, indicating its effective constraint satisfaction.

V. Conclusion

In this paper, we investigate the joint design of communication and sensing beamforming matrices in ISAC systems, where an optimization problem that maximizes the sensing performance under communication performance constraints is formulated. To this end, we propose a GNN-IP algorithm to solve the formulated MSE minimization problem, while reducing the computation complexity and guaranteeing the solution feasibility. Simulation results show that the proposed GNN-IP algorithm approaches the sensing MSE performance to the SDR algorithm while achieving much less computation complexity. The results also demonstrate the superiority of our proposed algorithm in guaranteeing the feasibility of the solution with respect to the DNN algorithm and the GNN only algorithm.

References

[1] F. Liu, Y. Cui, C. Masouros, J. Xu, T. X. Han, Y. C. Eldar, and S. Buzzi, "Integrated Sensing and Communications: Toward Dual-Functional Wireless Networks for 6G and Beyond," *IEEE J. Sel. Areas Commun.*, vol. 40, no. 6, pp. 1728–1767, 2022.

[2] A. Liu, Z. Huang, M. Li, Y. Wan, W. Li, T. X. Han, C. Liu, R. Du, D. K. P. Tan, J. Lu, Y. Shen, F. Colone, and K. Chetty, "A Survey on Fundamental Limits of Integrated Sensing and Communication," *IEEE Commun. Surveys Tuts.*, vol. 24, no. 2, pp. 994–1034, 2022.

[3] D. Wen, X. Li, Y. Zhou, Y. Shi, S. Wu, and C. Jiang, "Integrated sensing-communication-computation for edge artificial intelligence," *IEEE Commun. Sur. Tut., 2024.*, 2023.

[4] J. A. Zhang, F. Liu, C. Masouros, R. W. Heath, Z. Feng, L. Zheng, and A. Petropulu, "An Overview of Signal Processing Techniques for Joint Communication and Radar Sensing," *IEEE J. Sel. Topics Signal Process.*, vol. 15, no. 6, pp. 1295–1315, 2021.

[5] M. Roberton and E. Brown, "Integrated radar and communications based on chirped spread-spectrum techniques," in *IEEE MTT-S International Microwave Symposium Digest, 2003*, vol. 1, 2003, pp. 611–614 vol.1.

[6] G. N. Saddik, R. S. Singh, and E. R. Brown, "Ultra-Wideband Multifunctional Communications/Radar System," *IEEE Trans. Microw. Theory Techn.*, vol. 55, no. 7, pp. 1431–1437, 2007.

[7] E. BouDaher, A. Hassanien, E. Aboutanios, and M. G. Amin, "Towards a dual-function MIMO radar-communication system," in *IEEE Radar-Conf.*, 2016, pp. 1–6.

[8] M. F. Keskin, H. Wymeersch, and V. Koivunen, "MIMO-OFDM Joint Radar-Communications: Is ICI Friend or Foe?" *IEEE J. Sel. Topics Signal Process.*, vol. 15, no. 6, pp. 1393–1408, 2021.

[9] J. Johnston, L. Venturino, E. Grossi, M. Lops, and X. Wang, "MIMO OFDM Dual-Function Radar-Communication Under Error Rate and Beampattern Constraints," *IEEE J. Sel. Areas Commun.*, vol. 40, no. 6, pp. 1951–1964, 2022.

[10] F. Liu, C. Masouros, A. Li, H. Sun, and L. Hanzo, "MU-MIMO Communications With MIMO Radar: From Co-Existence to Joint Transmission," *IEEE Trans. Wireless Commun.*, vol. 17, no. 4, pp. 2755–2770, 2018.

[11] L. Chen, F. Liu, W. Wang, and C. Masouros, "Joint Radar-Communication Transmission: A Generalized Pareto Optimization Framework," *IEEE Trans. Signal Process.*, vol. 69, pp. 2752–2765, 2021.

[12] N. Huang, C. Dou, Y. Wu, L. Qian, B. Lin, H. Zhou, and X. Shen, "Mobile edge computing aided integrated sensing and communication with short-packet transmissions," *IEEE Trans. Wirel. Commun.*, pp. 1–1, 2023.

[13] D. Wen, P. Liu, G. Zhu, Y. Shi, J. Xu, Y. C. Eldar, and S. Cui, "Task-Oriented Sensing, Computation, and Communication Integration for Multi-Device Edge AI," *IEEE Trans. Wirel. Commun.*, vol. 23, no. 3, pp. 2486–2502, 2024.

[14] Y. LeCun, Y. Bengio, and G. Hinton, "Deep learning," *nature*, vol. 521, no. 7553, pp. 436–444, 2015.

[15] Y. Shi, L. Lian, Y. Shi, Z. Wang, Y. Zhou, L. Fu, L. Bai, J. Zhang, and W. Zhang, "Machine Learning for Large-Scale Optimization in 6G Wireless Networks," *IEEE Commun. Surv. Tut.*, vol. 25, no. 4, pp. 2088–2132, 2023.

[16] N. Cheng, F. Lyu, J. Chen, W. Xu, H. Zhou, S. Zhang, and X. Shen, "Big Data Driven Vehicular Networks," *IEEE Network*, vol. 32, no. 6, pp. 160–167, 2018.

[17] Y. Shi, Y. Zhou, D. Wen, Y. Wu, C. Jiang, and K. B. Letaief, "Task-oriented communications for 6g: Vision, principles, and technologies," *IEEE Wireless Commun. Mag.*, vol. 30, no. 3, pp. 78–85, 2023.

[18] Y. Xu, B. Qian, K. Yu, T. Ma, L. Zhao, and H. Zhou, "Federated Learning Over Fully-Decoupled RAN Architecture for Two-Tier Computing Acceleration," *IEEE J. Sel. Areas Commun.*, vol. 41, no. 3, pp. 789–801, 2023.

[19] Y. Zhou, Y. Shi, H. Zhou, J. Wang, L. Fu, and Y. Yang, "Toward Scalable Wireless Federated Learning: Challenges and Solutions," *IEEE Internet of Things Mag.*, vol. 6, no. 4, pp. 10–16, 2023.

[20] M. Tao, Y. Zhou, Y. Shi, J. Lu, S. Cui, J. Lu, and K. B. Letaief, "Federated Edge Learning for 6G: Foundations, Methodologies, and Applications," *Proc. IEEE*, pp. 1–39, 2024.

[21] C. Liu, W. Yuan, S. Li, X. Liu, H. Li, D. W. K. Ng, and Y. Li, "Learning-Based Predictive Beamforming for Integrated Sensing and Communication in Vehicular Networks," *IEEE J. Sel. Areas Commun.*, vol. 40, no. 8, pp. 2317–2334, 2022.

[22] Y. Zhao, Z. Wang, Z. Wang, X. Chen, and Y. Zhou, "Learning to Beamform for Dual-Functional MIMO Radar-Communication Systems," in *ICC 2023*, 2023, pp. 3572–3577.

[23] X. Liu, H. Zhang, K. Long, A. Nallanathan, and V. C. M. Leung, "Distributed Unsupervised Learning for Interference Management in Integrated Sensing and Communication Systems," *IEEE Trans. Wireless Commun.*, vol. 22, no. 12, pp. 9301–9312, 2023.

[24] Y. Shen, Y. Shi, J. Zhang, and K. B. Letaief, "Graph Neural Networks for Scalable Radio Resource Management: Architecture Design and Theoretical Analysis," *IEEE J. Sel. Areas Commun.*, vol. 39, no. 1, pp. 101–115, 2021.

[25] M. Eisen and A. Ribeiro, "Optimal Wireless Resource Allocation With Random Edge Graph Neural Networks," *IEEE Trans. Signal Process.*, vol. 68, pp. 2977–2991, 2020.

[26] T. Jiang, H. V. Cheng, and W. Yu, "Learning to Reflect and to Beamform for Intelligent Reflecting Surface With Implicit Channel Estimation," *IEEE Journal on Selected Areas in Communications*, vol. 39, no. 7, pp. 1931–1945, 2021.

[27] S. W. Golomb and G. Gong, *Signal design for good correlation for wireless communication, cryptography, and radar*. Cambridge University Press, 2005.

[28] D. Sarwate and M. Pursley, "Crosscorrelation properties of pseudorandom and related sequences," *Proc. IEEE*, vol. 68, no. 5, pp. 593–619, 1980.

[29] E. H. Kim and K. H. Kim, "Random phase code for automotive mimo radars using combined frequency shift keying-linear fmcw waveform," *IET Radar, Sonar & Navigation*, vol. 12, no. 10, pp. 1090–1095, 2018.

[30] C. Liao, F. Wang, and V. K. N. Lau, "Optimized Design for IRS-Assisted Integrated Sensing and Communication Systems in Clutter Environments," *IEEE Trans. Commun.*, vol. 71, no. 8, pp. 4721–4734, 2023.

[31] X. Shao, C. You, W. Ma, X. Chen, and R. Zhang, "Target Sensing With Intelligent Reflecting Surface: Architecture and Performance," *IEEE J. Sel. Areas Commun.*, vol. 40, no. 7, pp. 2070–2084, 2022.

[32] P. Stoica, J. Li, and Y. Xie, "On Probing Signal Design For MIMO Radar," *IEEE Trans. Signal Process.*, vol. 55, no. 8, pp. 4151–4161, 2007.

[33] X. Liu, T. Huang, N. Shlezinger, Y. Liu, J. Zhou, and Y. C. Eldar, "Joint Transmit Beamforming for Multiuser MIMO Communications and MIMO Radar," *IEEE Trans. Signal Process.*, vol. 68, pp. 3929–3944, 2020.

[34] F. Liu, Y.-F. Liu, A. Li, C. Masouros, and Y. C. Eldar, "Cramér-Rao Bound Optimization for Joint Radar-Communication Beamforming," *IEEE Trans. Signal Process.*, vol. 70, pp. 240–253, 2022.

[35] H. Luo, R. Liu, M. Li, Y. Liu, and Q. Liu, "Joint Beamforming Design for RIS-Assisted Integrated Sensing and Communication Systems," *IEEE Trans. Veh. Technol.*, vol. 71, no. 12, pp. 13 393–13 397, 2022.

[36] J. Li and P. Stoica, "MIMO Radar with Colocated Antennas," *IEEE Signal Process. Mag.*, vol. 24, no. 5, pp. 106–114, 2007.

[37] D. P. Palomar and Y. C. Eldar, *Convex optimization in signal processing and communications*. Cambridge university press, 2010.

[38] Z.-q. Luo, W.-k. Ma, A. M.-c. So, Y. Ye, and S. Zhang, "Semidefinite Relaxation of Quadratic Optimization Problems," *IEEE Signal Process. Mag.*, vol. 27, no. 3, pp. 20–34, 2010.

[39] X. Zhang, H. Zhao, J. Xiong, X. Liu, L. Zhou, and J. Wei, "Scalable Power Control/Beamforming in Heterogeneous Wireless Networks with Graph Neural Networks," in *2021 IEEE GLOBECOM*, 2021, pp. 01–06.

[40] Z. Wang, Y. Zhou, Y. Zou, Q. An, Y. Shi, and M. Bennis, "A Graph Neural Network Learning Approach to Optimize RIS-Assisted Federated Learning," *IEEE Trans. Wireless Commun.*, vol. 22, no. 9, pp. 6092–6106, 2023.

[41] S. Wan, Z. Wang, and Y. Zhou, "Scalable Hybrid Beamforming for Multi-User MISO Systems: A Graph Neural Network Approach," *IEEE Trans. Wireless Commun.*, pp. 1–1, 2024.

[42] K. Xu, W. Hu, J. Leskovec, and S. Jegelka, "How powerful are graph neural networks?" *arXiv preprint arXiv:1810.00826*, 2018.

[43] Z. Wu, S. Pan, F. Chen, G. Long, C. Zhang, and P. S. Yu, "A Comprehensive Survey on Graph Neural Networks," *IEEE Trans. Neural Netw. Learn. Syst.*, vol. 32, no. 1, pp. 4–24, 2021.

[44] K. Xu, C. Li, Y. Tian, T. Sonobe, K.-i. Kawarabayashi, and S. Jegelka, "Representation Learning on Graphs with Jumping Knowledge Networks," in *Proc. 35th Int. Conf. Mach. Learn. (ICML)*, ser. Proc. Mach. Learn. Res., J. Dy and A. Krause, Eds., vol. 80. PMLR, 10–15 Jul 2018, pp. 5453–5462. [Online]. Available: https://proceedings.mlr.press/v80/xu18c.html

[45] A. Agrawal, B. Amos, S. Barratt, S. Boyd, S. Diamond, and J. Z. Kolter, "Differentiable Convex Optimization Layers," *Adv. Neural Inf. Process. Syst.*, vol. 32, 2019.

[46] B. Amos and J. Z. Kolter, "OptNet: Differentiable Optimization as a Layer in Neural Networks," in *Proc. 34th Int. Conf. Mach. Learn. (ICML)*, ser. Proc. Mach. Learn. Res., D. Precup and Y. W. Teh, Eds., vol. 70. PMLR, 06–11 Aug 2017, pp. 136–145.

[47] M. Grant and S. Boyd, "CVX: Matlab software for disciplined convex programming, version 2.1," 2014.

[48] A. Paszke, S. Gross, F. Massa, A. Lerer, J. Bradbury, G. Chanan, T. Killeen, Z. Lin, N. Gimelshein, L. Antiga *et al.*, "PyTorch: An Imperative Style, High-Performance Deep Learning Library," in *Adv. Neural Inf. Process. Syst. (NeurIPS)*, vol. 32. Curran Associates, Inc., 2019.

[49] D. P. Kingma and J. Ba, "Adam: A method for stochastic optimization," *arXiv preprint arXiv:1412.6980*, 2014.

[50] M. C. Grant and S. P. Boyd, "Graph Implementations for Nonsmooth Convex Programs," in *Recent Adv. Learn. Control*, V. D. Blondel, S. P. Boyd, and H. Kimura, Eds. London: Springer London, 2008, pp. 95–110.

[51] R. H. Tütüncü, K.-C. Toh, and M. J. Todd, "Solving semidefinite-quadratic-linear programs using sdpt3," *Mathematical programming*, vol. 95, pp. 189–217, 2003.

[52] B. S. Khan, S. Jangsher, A. Ahmed, and A. Al-Dweik, "URLLC and eMBB in 5G Industrial IoT: A Survey," *IEEE Open J. Commun. Soc.*, vol. 3, pp. 1134–1163, 2022.

Yifei Zhao received the B.S. degree from the School of Information Science and Technology, ShanghaiTech University, Shanghai, China, in 2021. He is currently pursuing the Ph.D. degree with the School of Information Science and Technology, ShanghaiTech University, Shanghai, China. His research interests include machine learning and integrated sensing and communication.

Yong Zhou (Senior Member, IEEE) received the B.Sc. and M.Eng. degrees from Shandong University, Jinan, China, in 2008 and 2011, respectively, and the Ph.D. degree from the University of Waterloo, ON, Canada, in 2015. From Nov. 2015 to Jan. 2018, he worked as a postdoctoral researcher fellow in the Department of Electrical and Computer Engineering, The University of British Columbia, Vancouver, Canada. Since Mar. 2018, he has been with the School of Information Science and Technology, ShanghaiTech University, Shanghai, China, where he is currently a Tenured Associate Professor. He serves as an Associate Editor of IEEE Transactions on Wireless Communications and IEEE Open Journal of the Communications Society. He was the track co-chair of IEEE VTC 2020 Fall and IEEE VTC 2023 Spring, and the co-chair of IEEE ICC 2022 workshop on edge artificial intelligence for 6G and IEEE Globecom 2024 workshop on space computing power networks. His research interests include 6G communications, edge intelligence, and Internet of Things.

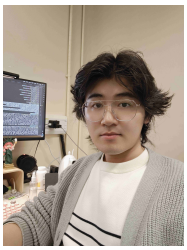

Zixin Wang (Member, IEEE) received the B.S. degree from Wuhan University of Technology, Wuhan, China, in 2018, and the Ph.D. degree from the University of Chinese Academy of Sciences, Shanghai, China, in 2024. Since March 2024, he has been working as a Postdoctoral Fellow with The Hong Kong University of Science and Technology (HKUST), clearwater bay, Hong Kong SAR. He visited University of Oulu, Oulu, Finland, from November 2022 to December 2023. His research interests include optimization, machine learning, wireless communications, and their applications to 6G and edge AI.

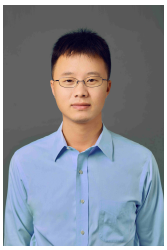

Yuanming Shi (Senior Member, IEEE) received the B.S. degree in electronic engineering from Tsinghua University, Beijing, China, in 2011. He received the Ph.D. degree in electronic and computer engineering from The Hong Kong University of Science and Technology (HKUST), in 2015. Since September 2015, he has been with the School of Information Science and Technology in ShanghaiTech University, where he is a Full Professor. He visited University of California, Berkeley, CA, USA, from October 2016 to February 2017. His research areas include edge artificial intelligence and large-scale optimization. He is a recipient of the IEEE Marconi Prize Paper Award in Wireless Communications in 2016, the Young Author Best Paper Award by the IEEE Signal Processing Society in 2016, the IEEE ComSoc Asia-Pacific Outstanding Young Researcher Award in 2021, the Chinese Institute of Electronics First Prize in Natural Science in 2022, and the China Institute of Communications First Prize in Natural Science in 2024. He is also an editor of IEEE Transactions on Wireless Communications, IEEE Journal on Selected Areas in Communications, Journal of Communications and Information Networks, and Space Habitation. He is an IET Fellow.

Nan Cheng (Senior Member, IEEE) received the Ph.D. degree in Electrical and Computer Engineering from the University of Waterloo in 2016, and B.E. degree and the M.S. degree in Information and Telecommunications Engineering from Tongji University in 2009 and 2012, respectively. He worked as a Post-doctoral fellow with the Department of Electrical and Computer Engineering, University of Toronto, from 2017 to 2019. He is currently a professor with State Key Lab. of ISN and with School of Telecommunications Engineering, Xidian University, Shaanxi, China. He has published over 110 journal papers in IEEE Transactions and other top journals. He serves as steering committee member of IEEE Journal on Miniaturization for Air and Space Systems, associate editors for IEEE Internet of Things Journal, IEEE Transactions on Vehicular Technology, IEEE Open Journal of the Vehicular Technology, and Peer-to-Peer Networking and Applications, and serves/served as guest editors for several journals. His current research focuses on B5G/6G, AI-driven future networks, and space-air-ground integrated network.

Haibo Zhou (Senior Member, IEEE) received the Ph.D. degree in information and communication engineering from Shanghai Jiao Tong University, Shanghai, China, in 2014. From 2014 to 2017, he was a Postdoctoral Fellow with the Broadband Communications Research Group, Department of Electrical and Computer Engineering, University of Waterloo. He is currently a Full Professor with the School of Electronic Science and Engineering, Nanjing University, Nanjing, China. He was a recipient of the 2019 IEEE ComSoc Asia-Pacific Outstanding Young Researcher Award. He served as Track/Symposium Co-Chair for IEEE/CIC ICCC 2019, IEEE VTC-Fall 2020, IEEE VTC-Fall 2021, and IEEE GLOBECOM 2022. He is currently an Associate Editor of the IEEE Transactions on Wireless Communications, IEEE Internet of Things Journal, IEEE Network Magazine, and IEEE Wireless Communications Letter. His research interests include resource management and protocol design in B5G/6G networks, vehicular ad hoc networks, and space-air-ground integrated networks.